

Call for participation: Verification benchmarks for single-phase flow in three-dimensional fractured porous media

Inga Berre^{1,5}, Wietse Boon², Bernd Flemisch^{2,*}, Alessio Fumagalli¹, Dennis Gläser², Eirik Keilegavlen¹, Anna Scotti³, Ivar Stefansson¹, and Alexandru Tatomir⁴

¹Department of Mathematics, University of Bergen, Allégaten 41, 5007 Bergen, Norway

²Department of Hydromechanics and Modelling of Hydrosystems, University of Stuttgart, Pfaffenwaldring 61, 70569 Stuttgart, Germany

³Laboratory for Modeling and Scientific Computing MOX, Politecnico di Milano, p.za Leonardo da Vinci 32, 20133 Milano, Italy

⁴Department of Applied Geology, Geosciences Center, University of Göttingen, Goldschmidtstrasse 3, 37077 Göttingen, Germany

⁵Christian Michelsen Research, Bergen, Norway

*bernd@iws.uni-stuttgart.de

ABSTRACT

This call for participation proposes four benchmark tests to verify and compare numerical schemes to solve single-phase flow in fractured porous media. With this, the two-dimensional suite of benchmark tests presented by Flemisch et al.¹ is extended to include three-dimensional problems. Moreover, transport simulations are included as a means to compare discretization methods for flow. With this publication, we invite researchers to contribute to the study by providing results to the test cases based on their applied discretization methods.

1 Introduction

In this call for participation, we propose four benchmark cases for the verification of computational models for single-phase flow in three-dimensional, fractured porous media. It can be seen as an extension of¹, where only two-dimensional test cases were considered. The current proposal also presents benchmarks where simulations of linear tracer transport are used as a means to compare flow discretizations. However, the process of collecting and comparing results is different. While the publication¹ contains both the case descriptions and a comparison of several computational models, this time we aim for a two-stage process. In particular, the present document describes the benchmark cases and serves as a call for participation to the interested scientific community. After a phase of collection and discussion of the results among the participants, we aim for a second publication that presents a comparison of the participating models. The case descriptions are accompanied by data in form of geometry descriptions, simulation results and plotting scripts, all available in the Git repository <https://git.iws.uni-stuttgart.de/benchmarks/fracture-flow-3d.git>. While access to this repository will be restricted to the benchmark participants during the phase of collection and comparison of the results, all data will be made publicly available upon submission of the comparison publication.

The rest of this document is organized as follows. In Section 2, we describe the mathematical models for fluid flow and transport in fractured porous media. Section 3 briefly describes the participating discretizations proposed by the authors as well as the discretization of the transport problem. Four test cases are introduced in Section 4 in form of domain and boundary condition descriptions as well as pointers to the relevant data in the Git repository. The final Section 5 provides instructions on how to participate in the benchmark study.

2 Mathematical models

We introduce two models for flow and transport in fractured media. First, the flow model is presented in the conventional, equi-dimensional setting, allowing for a natural introduction to the physical parameters. From this formulation, we derive the mixed-dimensional model through appropriate reduction of the equations. Note that the mixed-dimensional model forms the focus of this study. Finally, we introduce the equi- and mixed-dimensional transport models.

2.1 The equi-dimensional flow model

We consider a steady-state incompressible single-phase flow through a porous medium assumed to be described by Darcy's law, resulting in the governing system of equations

$$\begin{aligned} \mathbf{u} + \mathbb{K}\nabla h &= 0, \\ \nabla \cdot \mathbf{u} &= q, \end{aligned} \quad \text{in } \Lambda. \quad (1a)$$

Here, \mathbf{u} denotes the macroscopic fluid velocity in m/s whereas \mathbb{K} and h stand for hydraulic conductivity and pressure head measured in m/s and m, respectively; q represents a source/sink term measured in 1/s, and the regular domain $\Lambda \subset \mathbb{R}^3$ will be called the equi-dimensional domain. Coupled to (1a), we consider boundary conditions on the boundary $\partial\Lambda$ of Λ , namely

$$\begin{aligned} h|_{\partial\Lambda_h} &= \bar{h} & \text{on } \partial\Lambda_h, \\ \mathbf{u} \cdot \mathbf{n}|_{\partial\Lambda_u} &= \bar{u} & \text{on } \partial\Lambda_u. \end{aligned} \quad (1b)$$

We assume $\partial\Lambda = \partial\Lambda_h \cup \partial\Lambda_u$, $\partial\Lambda_h \cap \partial\Lambda_u = \emptyset$, and $|\partial\Lambda_h| > 0$. In (1b) $\cdot|_A$ is a suitable trace operator on $A \subset \partial\Lambda$, depending on the quantity at hand. Also, \bar{h} indicates the pressure head imposed on the boundary $\partial\Lambda_h$, while \bar{u} is the prescribed Darcy velocity normal to the boundary $\partial\Lambda_u$ with respect to the outer unit normal vector \mathbf{n} .

Problem (1) can be recast in its primal formulation, obtaining the equations

$$\begin{aligned} -\nabla \cdot \mathbb{K}\nabla h &= q & \text{in } \Lambda, \\ h|_{\partial\Lambda_h} &= \bar{h} & \text{on } \partial\Lambda_h, \\ -\mathbb{K}\nabla h \cdot \mathbf{n}|_{\partial\Lambda_u} &= \bar{u} & \text{on } \partial\Lambda_u. \end{aligned} \quad (2)$$

Problem (1) and (2) are equivalent, however, different numerical schemes are based on either of the two formulations. Under regularity assumptions on Λ and the data, the previous problems admit a unique weak solution. We refer to²⁻⁵ for more details.

We assume that Λ contains several fractures, i.e., inclusions in the domain. The fracture walls are considered planar and smooth, and the fractures have two distinguishing features: (1) The fracture thickness, which we measure by the aperture, denoted by ε , is small compared to the extension of the fracture. (2) The fracture hydraulic conductivity may differ significantly from that of the rest of Λ , implying that the fractures may have significant impact on the flow in Λ .

We furthermore make the assumption that the principal directions of the local hydraulic conductivities are aligned with the orientation of the fractures. In particular, the hydraulic conductivity in the matrix (\mathbb{K}_3), the fractures (\mathbb{K}_2), as well as in the intersections between two fractures (\mathbb{K}_1) and at the crossings of intersections (\mathbb{K}_0), can be decomposed in the following way:

$$\mathbb{K}_3 = K_3^{eq}, \quad \mathbb{K}_2 = \begin{bmatrix} K_2^{eq} & 0 \\ 0 & 0 & \kappa_2^{eq} \end{bmatrix}, \quad \mathbb{K}_1 = \begin{bmatrix} K_1^{eq} & 0 & 0 \\ 0 & \kappa_1^{eq} & 0 \\ 0 & 0 & \kappa_1^{eq} \end{bmatrix}, \quad \mathbb{K}_0 = \begin{bmatrix} \kappa_0^{eq} & 0 & 0 \\ 0 & \kappa_0^{eq} & 0 \\ 0 & 0 & \kappa_0^{eq} \end{bmatrix}. \quad (3)$$

Here, K_d^{eq} and κ_d^{eq} , for different values of d , denote the tangential and normal hydraulic conductivity, respectively. Thus, K_d^{eq} is an elliptic ($d \times d$)-tensor function whereas κ_d^{eq} is a positive scalar function. Note that the subscript d indicates that the features will be represented by d -dimensional objects in the reduced model, as derived in the next section. The superscript eq , on the other hand, indicates that these quantities are related to the equi-dimensional model.

2.2 Mixed-dimensional flow model

The small aperture of the fractures justifies a reduction of dimensionality procedure to Λ where fractures and their intersections are approximated by lower-dimensional objects. For more details on the derivation refer to⁶⁻¹⁵.

Here, we use Ω to denote the mixed-dimensional decomposition of Λ . Let Ω with outer boundary $\partial\Omega$ be composed of a possibly unconnected 3-dimensional domain Ω_3 which represents the rock matrix. Furthermore, Ω contains up to 3 lower-dimensional, open subdomains, namely the fracture planes Ω_2 , their intersection lines Ω_1 and intersection points Ω_0 . For compatibility, we assume that $\Omega_d \not\subset \Omega_{d'}$ for all $d' > d$. Finally, we introduce $\Gamma_d = \Omega_d \cap \partial\Omega_{d+1}$ as the set of d -interfaces between inter-dimensional sub-domains Ω_d and Ω_{d+1} endowed with a normal unit vector \mathbf{n} pointing outward from Ω_{d+1} .

Remaining consistent with the notation convention above, data and unknowns will also be annotated with a subscript related to the dimension. As a first example, on a d -dimensional feature $\Omega_{d,i} \subseteq \Omega_d$ with counting index i , let $\varepsilon_{d,i}$ denote the cross-sectional volume, area, or length of the corresponding physical domain for $d = 0, \dots, 2$ respectively. It naturally has the unit of measure m^{3-d} and is extended as non-dimensional unity in Ω_3 . Moreover, we introduce for each d -feature with index i , a typical length $a_{d,i}$ such that $\varepsilon_{d,i} = a_{d,i}^{3-d}$. In the continuation, we will omit the subscript i if no ambiguity arises.

We continue this subsection by first presenting the reduced model associated with (1) in the two-dimensional fractures Ω_2 followed by its generalization for all $d = 0, \dots, 3$.

2.2.1 Two-dimensional fracture flow

The primary variables in this formulation are the velocity $\mathbf{u}_3 = \mathbf{u}$ and hydraulic head $h_3 = h$ in the rock matrix Ω_3 , as well as the integrated, tangential velocity \mathbf{u}_2 and average hydraulic head h_2 in the fracture. These are given pointwise for $x \in \Omega_2$ by

$$\mathbf{u}_2(x) = \int_{\varepsilon_2(x)} \mathbf{u}_{\parallel} \quad \text{and} \quad h_2(x) = \frac{1}{\varepsilon_2(x)} \int_{\varepsilon_2(x)} h.$$

Here, \mathbf{u}_{\parallel} denotes the components of \mathbf{u} tangential to Ω_2 . The integrals are computed in the normal direction of the fracture and thus the corresponding units of measurement are m^2/s and m for \mathbf{u}_2 and h_2 , respectively.

Let us derive the reduced Darcy's law by averaging and the mass balance equation by integration over the direction normal to the fractures. Recall that the vector \mathbf{n} here refers to the normal unit vector pointing from Ω_3 into Ω_2 .

$$\begin{aligned} \frac{1}{\varepsilon_2} \mathbf{u}_2 + K_2^{eq} \nabla_2 h_2 &= 0 & \text{in } \Omega_2, \\ \nabla_2 \cdot \mathbf{u}_2 - \llbracket \mathbf{u}_3 \cdot \mathbf{n} \rrbracket &= q_2 \end{aligned} \quad (4a)$$

with ∇_2 the del-operator in the tangential directions and q_2 representing the integrated source term, i.e. $q_2(s) = \int_{\varepsilon_2(s)} q$. Note that here, we have assumed K_2^{eq} to be constant in the direction normal to Ω_2 . The jump operator is defined as $\llbracket \mathbf{u}_3 \cdot \mathbf{n} \rrbracket|_{\Omega_d} = \sum (\mathbf{u}_3 \cdot \mathbf{n}|_{\Gamma_2})$, therewith representing the mass exchange between fracture and matrix. In particular, for each subdomain $\Omega_{2,i} \subseteq \Omega_2$, we sum over all flux contributions over sections of Γ_2 which coincide geometrically with $\Omega_{2,i}$. These fluxes are assumed to satisfy the following Darcy-type law given by a finite difference between the hydraulic head in Ω_2 and on Γ_2 :

$$\mathbf{u}_3 \cdot \mathbf{n} + \kappa_2^{eq} \frac{2}{a_d} (h_2 - h_3) = 0 \quad \text{on } \Gamma_2. \quad (4b)$$

Note that to be mathematically precise, each term in this equation represents an appropriate trace or projection of the corresponding variable onto Γ_2 .

2.2.2 Generalized flow model

Next, we generalize the equations described above to domains of all dimensions, thus including the intersection lines and points. For that purpose, we introduce the integrated velocity \mathbf{u}_d for $d = 1$ and average hydraulic head h_d with $d = 0, 1$ given pointwise for $x \in \Omega_d$ by

$$\mathbf{u}_1(x) = \int_{\varepsilon_1(x)} \mathbf{u}_{\parallel} \quad \text{and} \quad h_d(x) = \frac{1}{\varepsilon_d(x)} \int_{\varepsilon_d(x)} h, \quad \text{for } d = 0, 1.$$

Again, \mathbf{u}_{\parallel} denotes the components of \mathbf{u} tangential to Ω_1 . The integrals are computed in the directions normal to the intersection lines Ω_1 , and points Ω_0 . The corresponding units of measurement are therefore m^3/s and m for \mathbf{u}_1 and h_d , respectively. The analogues of (4a) on these lower-dimensional manifolds are then given by

$$\begin{aligned} \frac{1}{\varepsilon_1} \mathbf{u}_1 + K_1^{eq} \nabla_1 h_1 &= 0 \\ \nabla_1 \cdot \mathbf{u}_1 - \llbracket \mathbf{u}_2 \cdot \mathbf{n} \rrbracket &= q_1 & \text{in } \Omega_1, \\ - \llbracket \mathbf{u}_1 \cdot \mathbf{n} \rrbracket &= q_0 & \text{in } \Omega_0. \end{aligned} \quad (5)$$

Here, ∇_1 denotes the del-operator, i.e. the derivative, in Ω_1 . Moreover, the linear jump operator $\llbracket \cdot \rrbracket$ is naturally generalized to $\llbracket \mathbf{u}_{d+1} \cdot \mathbf{n} \rrbracket|_{\Omega_d} = \sum (\mathbf{u}_{d+1} \cdot \mathbf{n}|_{\Gamma_d})$, where we for each subdomain $\Omega_{d,i} \subseteq \Omega_d$ sum over all flux contributions over sections of Γ_d which coincide geometrically with $\Omega_{d,i}$. Finally q_1 and q_0 correspond to the integrated source terms in the intersection lines and points, respectively.

Due to our choice of defining \mathbf{u}_d as the integrated velocity, a scaling with ε_{d+1} appears in the equation governing the flux across Γ_d :

$$\frac{1}{\varepsilon_{d+1}} \mathbf{u}_{d+1} \cdot \mathbf{n} + \kappa_d^{eq} \frac{2}{a_d} (h_d - h_{d+1}) = 0 \quad \text{on } \Gamma_d, \quad d = 0, 1. \quad (6)$$

Recalling that $\varepsilon_3 = 1$, it now follows that the effective tangential and normal hydraulic conductivities are given by:

$$K_d = \varepsilon_d K_d^{eq}, \quad \text{in } \Omega_d, \quad d = 1, \dots, 3 \quad (7a)$$

$$\kappa_d = \varepsilon_{d+1} \frac{2}{a_d} \kappa_d^{eq}, \quad \text{on } \Gamma_d, \quad d = 0, \dots, 2. \quad (7b)$$

From these definitions, it is clear that the units of K_d and κ_d are m^{4-d}/s and m^{2-d}/s , respectively.

Collecting the above equations, we obtain the generalization of system (4) to subdomains of all dimensions. The resulting system consists of Darcy's law in both tangential and normal directions followed by the mass conservation equations:

$$\begin{aligned} \mathbf{u}_d + K_d \nabla_d h_d &= 0, & \text{in } \Omega_d, d = 1, \dots, 3, & \quad (8a) \\ \mathbf{u}_{d+1} \cdot \mathbf{n} + \kappa_d (h_d - h_{d+1}) &= 0, & \text{on } \Gamma_d, d = 0, \dots, 2, & \quad (8b) \\ \nabla_d \cdot \mathbf{u}_3 &= q_3, & \text{in } \Omega_3, & \quad (8c) \\ \nabla_d \cdot \mathbf{u}_d - \llbracket \mathbf{u}_{d+1} \cdot \mathbf{n} \rrbracket &= q_d, & \text{in } \Omega_d, d = 1, 2, & \quad (8d) \\ -\llbracket \mathbf{u}_1 \cdot \mathbf{n} \rrbracket &= q_0, & \text{in } \Omega_0. & \quad (8e) \end{aligned}$$

The source term is given by q_3 for the rock matrix and $q_d(x) = \int_{\varepsilon_d(x)} q$ measured in m^{3-d}/s .

The system (8) is then compactly described by:

$$\begin{aligned} \mathbf{u}_d + K_d \nabla_d h_d &= 0, & \text{in } \Omega_d, d = 1, \dots, 3, & \quad (9a) \\ \mathbf{u}_{d+1} \cdot \mathbf{n} + \kappa_d (h_d - h_{d+1}) &= 0, & \text{on } \Gamma_d, d = 0, \dots, 2, & \quad (9b) \\ \nabla_d \cdot \mathbf{u}_d - \llbracket \mathbf{u}_{d+1} \cdot \mathbf{n} \rrbracket &= q_d, & \text{in } \Omega_d, d = 0, \dots, 3. & \quad (9c) \end{aligned}$$

in which the non-physical \mathbf{u}_4 and \mathbf{u}_0 are understood as zero. The associated boundary conditions are inherited from the equidimensional model with the addition of a no-flux condition at embedded fracture endings:

$$\begin{aligned} h_d &= \bar{h} & \text{on } \partial\Omega_d \cap \partial\Lambda_h, d = 0, \dots, 3, & \quad (10a) \\ \mathbf{u}_d \cdot \mathbf{n} &= \varepsilon_d \bar{u} & \text{on } \partial\Omega_d \cap \partial\Lambda_u, d = 1, \dots, 3, & \quad (10b) \\ \mathbf{u}_d \cdot \mathbf{n} &= 0 & \text{on } \partial\Omega_d \setminus (\Gamma_{d-1} \cup \partial\Lambda), d = 1, \dots, 3. & \quad (10c) \end{aligned}$$

To finish the section, we present the primal formulation of the mixed-dimensional fracture flow model. In analogy with (2), this formulation is derived by substituting the Darcy's laws (9a), (9b) into the conservation equation (9c):

$$-\nabla_d \cdot K_d \nabla_d h_d + \llbracket \kappa_d (h_d - h_{d+1}) \rrbracket = q_d, \quad \text{in } \Omega_d, d = 0, \dots, 3. \quad (11)$$

In this case, we set the divergence term to zero if $d = 0$ and the jump term to zero if $d = 3$. The boundary conditions are given by

$$\begin{aligned} h_d &= \bar{h} & \text{on } \partial\Omega_d \cap \partial\Lambda_h, d = 0, \dots, 3, & \quad (12a) \\ -K_d \nabla_d h_d \cdot \mathbf{n} &= \varepsilon_d \bar{u} & \text{on } \partial\Omega_d \cap \partial\Lambda_u, d = 1, \dots, 3, & \quad (12b) \\ -K_d \nabla_d h_d \cdot \mathbf{n} &= 0 & \text{on } \partial\Omega_d \setminus (\Gamma_{d-1} \cup \partial\Lambda), d = 1, \dots, 3. & \quad (12c) \end{aligned}$$

Many discretization schemes of the mixed-dimensional model described here, ignore flow in one-dimensional fracture intersections and zero-dimensional intersections thereof. Although these correspond to discretizing a simpler model, this is perfectly in line with the proposed study. In particular, it will be interesting to evaluate differences in the results that can be attributed to whether these lower-dimensional intersections are included in the model, and therewith the discretization, or not.

2.3 Equi-dimensional transport model

We now consider a scalar quantity c with the unit of measure m^{-3} , which is transported through the porous medium subject to the velocity field resulting from the flow model presented in the previous sections. The purely advective transport of c is described by the conservation equation:

$$\phi \frac{\partial c}{\partial t} + \nabla \cdot (c\mathbf{u}) = q_c \quad \text{in } \Lambda, \quad (13)$$

where ϕ is the porosity of the porous medium and q_c is a source/sink term for c given in m^{-3}/s . We define Dirichlet boundary conditions on those boundary segments where inflow occurs, i.e.:

$$c|_{\partial\Lambda_c} = \bar{c} \quad \text{on } \partial\Lambda_c, \quad \partial\Lambda_c = \{x \in \partial\Lambda : \mathbf{u} \cdot \mathbf{n} < 0\}, \quad (14)$$

with \bar{c} being the value for c prescribed on the boundary $\partial\Lambda_c$.

2.4 Mixed-dimensional transport model

In analogy to Section 2.2, we choose the average value for c as primary variable, which is defined as $c_3 = c$ in Ω_3 and for the lower dimensional objects (with $d \leq 2$) as

$$c_d(s) = \frac{1}{\varepsilon_d(s)} \int_{\varepsilon_d(s)} c.$$

Following the derivation of the mixed-dimensional flow model presented in Section 2.2, the resulting mixed-dimensional transport model reads:

$$\varepsilon_d \phi_d \frac{\partial c_d}{\partial t} + \nabla_d \cdot (c_d \mathbf{u}_d) - \llbracket \tilde{c}_{d+1} (\mathbf{u}_{d+1} \cdot \mathbf{n}) \rrbracket = q_{c,d} \quad \text{in } \Omega_d, \quad d = 0, \dots, 3. \quad (15)$$

Note that for $d = 0$, the divergence term is void. Here, the porosity is simply $\phi_d = \phi^{eq}$, with unit of measure m^{-3} , and \tilde{c}_{d+1} is evaluated on the basis of a first order upwind scheme, i.e.:

$$\tilde{c}_{d+1} = \begin{cases} c_{d+1} & \text{if } \mathbf{u}_{d+1} \cdot \mathbf{n}|_{\Gamma_d} > 0 \\ c_d & \text{if } \mathbf{u}_{d+1} \cdot \mathbf{n}|_{\Gamma_d} < 0. \end{cases} \quad (16)$$

As in the flow model, the jump operator represents the sum of the fluxes over all contributions defined on sections of Γ_d that coincide geometrically with $\Omega_{d,i}$.

3 Discretization

The intent of the proposed benchmark study is to quantitatively evaluate different discretization schemes for the mixed-dimensional flow models (9), (10) and (11), (12). The transport models described above are employed as a means to further evaluate and compare results for different flow discretizations. In the repository, the authors have already uploaded results to the test cases based on the following methods:

1. **U_iB-TPFA**: Two-point flux approximation finite volume method (cell-centered pressure, conforming DFM grid, discontinuous over lower-dimensional features, mass transfer in intersection lines and points).
2. **U_iB-MPFA**: Multi-point flux approximation finite volume method (cell-centered pressure, conforming DFM grid, discontinuous over lower-dimensional features, mass transfer in intersection lines and points).
3. **U_iB-RT0**: Lowest order Raviart-Thomas mixed finite elements (cell-centered pressure and face flux, conforming DFM grid, discontinuous over lower-dimensional features, mass transfer in intersection lines and points).
4. **U_iB-MVEM**: Lowest order mixed virtual element method (cell-centered pressure and face flux, conforming DFM grid, discontinuous over lower-dimensional features, mass transfer in intersection lines and points).
5. **USTUTT-MPFA**: Multi-point flux approximation finite volume method (cell-centered pressure, conforming DFM grid, discontinuous over lower-dimensional features, *no* mass transfer in intersection lines and points).

Methods 1-4 are all implemented following the mixed-dimensional approach described in¹⁶.

To evaluate the fluxes produced by each discretization quantitatively, they are to be inserted into a standard cell-centered first-order-upwind scheme for the transport, together with the implicit Euler method for temporal discretization with a fixed time-step that will be prescribed for each test case.

4 Benchmark cases

In the next subsections we introduce the proposed benchmark cases. For each case, pressure and tracer concentration need to be computed along with several associated macroscopic metrics. In Subsection 4.1 a problem containing a single fracture problem is considered. Subsection 4.2 contains a synthetic network composed by 9 fractures. The example in Subsection 4.3 considers the geometrically challenging case of almost intersecting fractures, fractures with small intersections, and other features that a fracture network may exhibit. Finally, in Subsection 4.4 we study a selection of a few dozen fractures from a real network. In all the cases the purpose is to validate the performance of the proposed numerical schemes and model choices.

4.1 Case 1: single fracture

Description Figure 1 illustrates the first proposed benchmark example for testing the discrete fracture flow and transport models in three-dimensional space. The geometry of the system is slightly modified from the previous works of^{f17} and¹⁸. The domain, Ω , is a cube-shaped region $(0 \text{ m}, 100 \text{ m}) \times (0 \text{ m}, 100 \text{ m}) \times (0 \text{ m}, 100 \text{ m})$ which is crossed by a planar fracture, Ω_2 , with a thickness of $1 \times 10^{-2} \text{ m}$. The fracture divides the domain into the sub-domains $\Omega_{3,1}$ and $\Omega_{3,2}$. Furthermore, an additional sub-domain $\Omega_{3,3}$ is defined in the lower part of the domain, representing a heterogeneity within the rock matrix. Inflow into the system occurs through a narrow band defined by $\{0 \text{ m}\} \times (0 \text{ m}, 100 \text{ m}) \times (90 \text{ m}, 100 \text{ m})$. Similarly, the outlet is a narrow band defined by $(0 \text{ m}, 100 \text{ m}) \times \{0 \text{ m}\} \times (0 \text{ m}, 100 \text{ m})$. Except for the inlet and outlet bands, on which Dirichlet boundary conditions are set, all other boundaries are treated as no-flow boundaries. For the hydraulic head, $h_{in} = 4 \text{ m}$ and $h_{out} = 1 \text{ m}$ are set on the inlet and outlet boundaries, respectively, while for the transport $c_{in} = 1 \times 10^{-2} \text{ m}^{-3}$ is set at the inlet. The overall simulation time is $1 \times 10^9 \text{ s}$.

Parameters

Matrix hydraulic conductivity $K_{3,1}, K_{3,2}$	$1 \times 10^{-6} \mathbf{I}$	m/s
Matrix hydraulic conductivity $K_{3,3}$	$1 \times 10^{-5} \mathbf{I}$	m/s
Fracture effective tangential hydraulic conductivity K_2	$1 \times 10^{-3} \mathbf{I}$	m ² /s
Fracture effective normal hydraulic conductivity κ_2	20	1/s
Matrix porosity $\phi_{3,1}, \phi_{3,2}$	2×10^{-1}	
Matrix porosity $\phi_{3,3}$	2.5×10^{-1}	
Fracture porosity ϕ_2	4×10^{-1}	
Fracture cross-sectional length ε_2	1×10^{-2}	m

Folder in Git repository `single`

Results We consider a constant time step size $\Delta t = 10^7 \text{ s}$. The results of three different simulations with approximately 1k, 10k and 100k cells for the 3D domain are collected and the comparison among the different schemes is then done on the basis of the following results:

1. The number of cells and degrees of freedom, according to the guidelines described in Subsection 5.4 point 3, saved in the file `results.csv`;
2. the computation of $\int_{\Omega_{3,3}} \phi_3 c_3 dx$ for each time step;
3. the computation of $\int_{\Omega_2} \varepsilon_2 \phi_2 c_2 dx$ for each time step;
4. the integrated flux of c across the outlet boundary for each time step;
5. the plot of the hydraulic head h_3 in the matrix along the line $(0 \text{ m}, 100 \text{ m}, 100 \text{ m}) - (100 \text{ m}, 0 \text{ m}, 0 \text{ m})$;

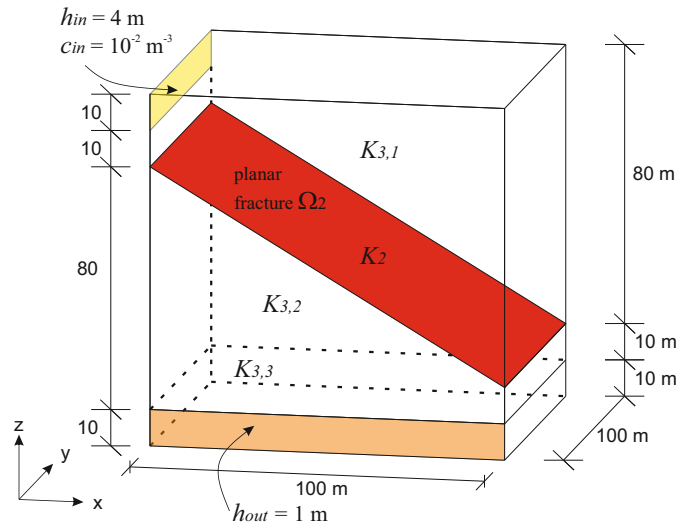


Figure 1. Conceptual model and geometrical description of the domain for test case of Subsection 4.1.

6. the plot of c_3 in the matrix, at the final simulation time, along the line (0 m, 100 m, 100 m)-(100 m, 0 m, 0 m);
7. the plot of c_2 within the fracture, at the final simulation time, along the line (0 m, 100 m, 80 m)-(100 m, 0 m, 20 m).

In files called `dot_refinement_${REFINEMENT}.csv` report the results ordered column-wise in the following way: time, result from point 2, 3, and 4. The variable `REFINEMENT` runs from 0 to 2 for increasing refinement. Similarly, in files called `dol_refinement_${REFINEMENT}.csv` report the results ordered in the following way: arc length and result from point 5, arc length and result from point 6, and arc length and result from point 7. See Subsection 5.4 for more details on how to report results.

4.2 Case 2: regular fracture network

Description The second benchmark is an extension of test case 4.1 from the benchmark study¹ in a 3D setting. The geometry is slightly modified from¹⁹ to allow a full 3D solution field. The unit cube domain is $\Omega = (0\text{ m}, 1\text{ m})^3$ and 9 fractures are present, see Appendix 6.1 for the coordinates. A graphical representation is given by Figure 2.

We define the portion of the boundary where we impose a non-homogeneous flux condition as $\partial\Omega_{flux}$ and choose $\partial\Omega_h = \{(x, y, z) \in \partial\Omega : x, y, z > 0.875\text{ m}\}$ and $\partial\Omega_{flux} = \{(x, y, z) \in \partial\Omega : x, y, z < 0.25\text{ m}\}$, respectively. On $\partial\Omega_h$ we impose $\bar{h} = 1\text{ m}$, while on $\partial\Omega_{flux}$ we impose $\bar{u} = -1\text{ m/s}$. On the rest of the boundary of Ω and on the lower-dimensional objects, we impose homogeneous flux conditions. Two test cases are considered: high-conductive fractures ($\mathcal{S}\{\text{COND}\} = 0$) and low-conductive fractures ($\mathcal{S}\{\text{COND}\} = 1$). We define the following matrix sub-regions

$$\Omega_{3,0} = \Omega_3 \setminus \Omega_{3,1}$$

$$\Omega_{3,1} = \{(x, y, z) \in \Omega_3 : x > 0.5\text{ m} \cap y < 0.5\text{ m}\}$$

$$\cup \{(x, y, z) \in \Omega_3 : x > 0.75\text{ m} \cap 0.5\text{ m} < y < 0.75\text{ m} \cap z > 0.5\text{ m}\}$$

$$\cup \{(x, y, z) \in \Omega_3 : 0.625\text{ m} < x < 0.75\text{ m} \cap 0.5\text{ m} < y < 0.625\text{ m} \cap 0.5\text{ m} < z < 0.75\text{ m}\},$$

see the right part of Figure 2, and prescribe two different matrix hydraulic conductivities.

For the transport problem, we impose unitary concentration at the inflow boundary and time interval equal to $[0, 0.25]\text{ s}$.

Parameters

	$\mathcal{S}\{\text{COND}\} = 0$	$\mathcal{S}\{\text{COND}\} = 1$
Matrix hydraulic conductivity $K_3 _{\Omega_{3,0}}$	\mathbf{I} m/s	\mathbf{I} m/s
Matrix hydraulic conductivity $K_3 _{\Omega_{3,1}}$	$1 \times 10^{-1}\mathbf{I}$ m/s	$1 \times 10^{-1}\mathbf{I}$ m/s
Fracture effective tangential hydraulic conductivity K_2	\mathbf{I} m ² /s	$1 \times 10^{-8}\mathbf{I}$ m ² /s
Fracture effective normal hydraulic conductivity κ_2	2×10^8 1/s	2 1/s
Intersection effective tangential hydraulic conductivity K_1	1×10^{-4} m ³ /s	1×10^{-12} m ³ /s
Intersection effective normal hydraulic conductivity κ_1	2×10^4 m/s	2×10^{-4} m/s
Intersection effective normal hydraulic conductivity κ_0	2 m ² /s	2×10^{-8} m ² /s
Matrix porosity ϕ_3	1×10^{-1}	1×10^{-1}
Fracture porosity ϕ_2	9×10^{-1}	1×10^{-2}
Intersection porosity ϕ_1	9×10^{-1}	1×10^{-2}
Fracture cross-sectional length ε_2	1×10^{-4} m	1×10^{-4} m
Intersection cross-sectional area ε_1	1×10^{-8} m ²	1×10^{-8} m ²
Intersection cross-sectional volume ε_0	1×10^{-12} m ³	1×10^{-12} m ³

Folder in Git repository `regular`

Results Results will be collected for a sequence of 3 simulations, by taking approximately 500, 4k, and 32k cells for the 3D domain. For the lower dimensional objects the number of cells should be chosen accordingly. The meshes may, if desirable, be obtained using the Gmsh mesh generator using the file `gmsh.geo` in the folder `regular/geometry` of the repository,

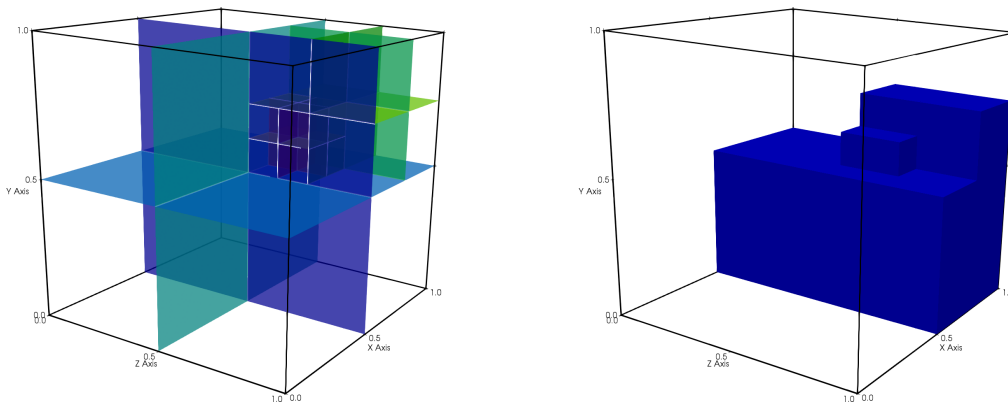


Figure 2. On the left, representation of the fractures and the outline of the domain for the test case of Subsection 4.2. On the right, the part of the rock matrix with low hydraulic conductivity $\Omega_{3,1}$.

where the mesh parameter h can vary in $[0.25, 0.12, 0.045]$ m. The time interval is divided in 100 equal time steps. The results to be reported are:

1. The number of cells and degrees of freedom, according to the guidelines described in in Subsection 5.4 point 3, saved in two files `results_cond- $\{COND\}$.csv`;
2. for each mesh, the plot of the matrix hydraulic head h_3 along the line from $(0, 0, 0)$ to $(1, 1, 1)$;
3. for the second level of mesh refinement, the average concentration on each matrix block during time. The average concentration is defined as $\int_{\Omega_{3,i}} c_3 / |\Omega_{3,i}| \text{m}^{-3}$, with i the region identifier.

In files called `dol_cond- $\{COND\}$ _refinement- $\{REFINEMENT\}$.csv` report the results from point 2. The variable $\{REFINEMENT\}$ runs from 0 to 2 for increasing refinement, while $\{COND\}$ should be 0 for the high-conductive case and 1 for low-conductive. For point 3, the sub-domain identification indexes *region_id* are defined in Appendix 6.1, and the file `color_regions.vtu` shows a graphical representation of these regions. The output is organised in the following way: two files named `dot_cond- $\{COND\}$.csv` having time as the first column, and the other columns the averaged concentration in each of the regions.

4.3 Case 3: network with small features

Description This test is designed to probe accuracy in the presence of small geometric features, that may cause trouble for conforming meshing strategies. The domain is a box $\Omega = (0\text{ m}, 1\text{ m}) \times (0\text{ m}, 2.25\text{ m}) \times (0\text{ m}, 1\text{ m})$, containing eight fractures. These are defined by their vertexes, given in Appendix 6.2, and the geometry is depicted in Figure 3. A Gmsh file `gmsh.geo` representing this geometry is uploaded to the Git repository in the folder `small_features/geometry`.

We define in and outlet boundaries as follows:

$$\partial\Omega_N = \partial\Omega \setminus (\partial\Omega_{in} \cup \partial\Omega_{out}) \quad \partial\Omega_{in} = (0\text{ m}, 1\text{ m}) \times \{0\text{ m}\} \times (1/3\text{ m}, 2/3\text{ m})$$

$$\partial\Omega_{out} = \partial\Omega_{out,0} \cup \partial\Omega_{out,1} \quad \partial\Omega_{out,0} = (0\text{ m}, 1\text{ m}) \times \{2.25\text{ m}\} \times (0\text{ m}, 1/3\text{ m})$$

$$\partial\Omega_{out,1} = (0\text{ m}, 1\text{ m}) \times \{2.25\text{ m}\} \times (2/3\text{ m}, 1\text{ m})$$

The boundary conditions for flow are: homogeneous Dirichlet conditions on $\partial\Omega_{out}$, uniform unit inflow on $\partial\Omega_{in}$, so that $\int_{\partial\Omega_{in}} \mathbf{u}_3 \cdot \mathbf{n} dS = -1/3 \text{ m}^3/\text{s}$, and homogeneous Neumann conditions on $\partial\Omega_N$. For the transport problem, we consider homogeneous initial conditions and as boundary condition a unit concentration at $\partial\Omega_{in}$. The overall simulation time is 1 s.

Parameters

Matrix hydraulic conductivity K_3	\mathbf{I}	m/s
Fracture effective tangential hydraulic conductivity K_2	$1 \times 10^2 \mathbf{I}$	m^2/s
Fracture effective normal hydraulic conductivity κ_2	2×10^6	1/s
Intersection effective tangential hydraulic conductivity K_1	1	m^3/s
Intersection effective normal hydraulic conductivity κ_1	2×10^4	m/s
Matrix porosity ϕ_3	2×10^{-1}	
Fracture porosity ϕ_2	2×10^{-1}	
Intersection effective porosity ϕ_1	2×10^{-1}	
Fracture cross-sectional length ε_2	1×10^{-2}	m
Intersection cross-sectional area ε_1	1×10^{-4}	m^2

Folder in Git repository `small_features`

Results The simulations should be done on 2 grids with approximately 30k and 150k 3D cells, labeled by $\$\{\text{REFINEMENT}\}$ 0 and 1, respectively. The time step size is $\Delta t = 1 \times 10^{-2}$ s. The results to be reported are:

1. The number of cells and degrees of freedom according to the guidelines described in Subsection 5.4 point 3 in a file named `results.csv`. In addition, the total outflow over $\partial\Omega_{out,0}$ and $\partial\Omega_{out,1}$ as columns seven and eight;
2. the average hydraulic head h_3 at the inlet, $\partial\Omega_{in}$, reported as column nine of `results.csv`. The interpretation of hydraulic head at the inlet faces may differ between numerical methods; this should be seen as part of the discretization.
3. the hydraulic head h_3 in the matrix along the line $(0.5\text{ m}, 1.1\text{ m}, 0\text{ m})$ - $(0.5\text{ m}, 1.1\text{ m}, 1\text{ m})$;
4. the hydraulic head h_3 in the matrix along $(0\text{ m}, 2.15\text{ m}, 0.5\text{ m})$ - $(1\text{ m}, 2.15\text{ m}, 0.5\text{ m})$;
5. the mean tracer concentrations for each fracture and time step.

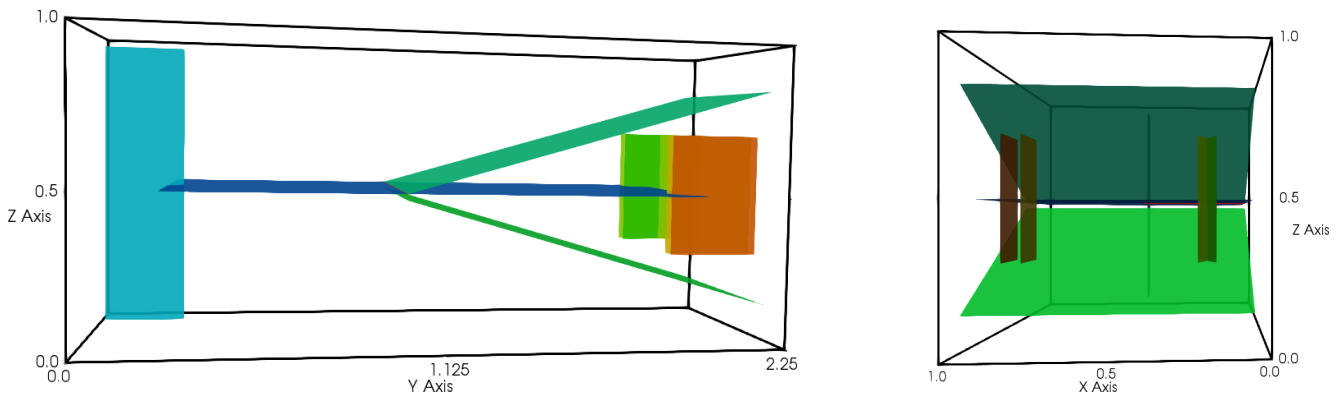


Figure 3. Representation of the fractures and the outline of the domain for the test case of Subsection 4.3.

In files called `dol_line- $\{LINE\}$ _refinement- $\{REFINEMENT\}$.csv` report the results from point 3 and 4, respectively for $\{LINE\} = 0$ and $\{LINE\} = 1$. For point 5, report in a file `dot_refinement- $\{REFINEMENT\}$.csv`, with time in the first column, followed by the eight mean values ordered as in Appendix 6.2.

4.4 Case 4: a field case

Description The fourth example has a geometry based on a post-processed outcrop from the island of Algeøyna, outside Bergen, Norway. From the outcrop, 52 fractures are selected, extruded in the vertical direction and then cut by a bounding box. The resulting fracture geometry is depicted in Figure 4. The resulting network has 106 fracture intersections, and multiple fractures intersecting the domain boundary.

The simulation domain is the box $\Omega = (-500\text{ m}, 350\text{ m}) \times (100\text{ m}, 1500\text{ m}) \times (-100\text{ m}, 500\text{ m})$. The polygons describing the fractures can be found in the file `fracture_network.csv` in the folder `field`. A Gmsh file `gmsh.geo` describing the fracture geometry is provided in the subfolder `field/geometry`. We define in and outlet boundaries as follows:

$$\begin{aligned}\partial\Omega_N &= \partial\Omega \setminus (\partial\Omega_{in} \cup \partial\Omega_{out}), & \partial\Omega_{in} &= \partial\Omega_{in,0} \cup \partial\Omega_{in,1}, & \partial\Omega_{out} &= \partial\Omega_{out,0} \cup \partial\Omega_{out,1}, \\ \partial\Omega_{in,0} &= (-500\text{ m}, -200\text{ m}) \times \{1500\text{ m}\} \times (300\text{ m}, 500\text{ m}), \\ \partial\Omega_{in,1} &= \{-500\text{ m}\} \times (1200\text{ m}, 1500\text{ m}) \times (300\text{ m}, 500\text{ m}), \\ \partial\Omega_{out,0} &= \{-500\text{ m}\} \times (100\text{ m}, 400\text{ m}) \times (-100\text{ m}, 100\text{ m}), \\ \partial\Omega_{out,1} &= \{350\text{ m}\} \times (100\text{ m}, 400\text{ m}) \times (-100\text{ m}, 100\text{ m}).\end{aligned}$$

The boundary conditions for flow are: homogeneous Dirichlet conditions on $\partial\Omega_{out}$, uniform unit inflow on $\partial\Omega_{in}$, so that $\int_{\partial\Omega_{in}} \mathbf{u}_3 \cdot \mathbf{n} dS = -1.2 \times 10^5 \text{ m}^3/\text{s}$, and homogeneous Neumann conditions on $\partial\Omega_N$. For the transport problem, we consider homogeneous initial conditions, with a unit concentration as boundary condition at $\partial\Omega_{in}$. The overall simulation time is $5 \times 10^3 \text{ s}$.

Parameters

Matrix hydraulic conductivity K_3	\mathbf{I}	m/s
Fracture effective tangential hydraulic conductivity K_2	$1 \times 10^2 \mathbf{I}$	m^2/s
Fracture effective normal hydraulic conductivity κ_2	2×10^6	1/s
Intersection effective tangential hydraulic conductivity K_1	1	m^3/s
Intersection effective normal hydraulic conductivity κ_1	2×10^4	m/s
Matrix porosity ϕ_3	2×10^{-1}	
Fracture porosity ϕ_2	2×10^{-1}	
Intersection porosity ϕ_1	2×10^{-1}	
Fracture cross-sectional length ε_2	1×10^{-2}	m
Intersection cross-sectional area ε_1	1×10^{-4}	m^2

Folder in Git repository `field`

Results We consider a time step size of $\Delta t = 50 \text{ s}$. The results to be reported are:

1. The number of cells and degrees of freedom according to the guidelines described in Subsection 5.4 point 3 in a file named `results.csv`. In addition, the total outflow over $\partial\Omega_{out,0}$ and $\partial\Omega_{out,1}$ as columns seven and eight;

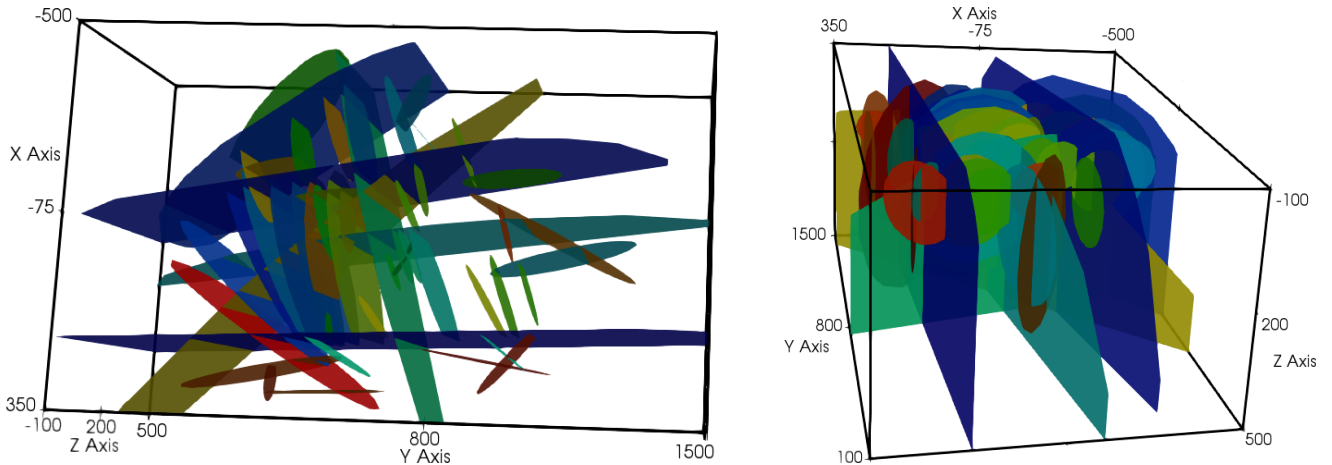


Figure 4. Representation of the fractures and the outline of the domain for the test case of Subsection 4.4.

2. the average hydraulic head h_3 at the inlet, $\partial\Omega_{in}$, reported as the seventh column of `results.csv`;
3. the hydraulic head h_3 in the matrix along $(350\text{m}, 100\text{m}, -100\text{m})-(-500\text{m}, 1500\text{m}, 500\text{m})$;
4. the hydraulic head h_3 in the matrix along $(-500\text{m}, 100\text{m}, -100\text{m})-(350\text{m}, 1500\text{m}, 500\text{m})$;
5. the mean tracer concentrations throughout the simulation time in all fractures.

In files called `do_line_${LINE}.csv` report the results from point 3 and 4, respectively for $\{LINE\} = 0$ and $\{LINE\} = 1$. For point 5, report in a file `dot.csv`, with time in the first column, followed by the 52 mean concentration values.

5 How to participate

We welcome all computational modelers to participate in the proposed benchmark study. Three different stages of participation can be identified: 1. registration, 2. simulation and synchronization, 3. publication. In the following, we will describe each stage in more detail.

5.1 Registration

If an interested researcher would like to participate in the benchmark study, he/she should fill in the Google form provided at <https://goo.gl/forms/wCaPLipPIld5Qz1j1>. One form should be submitted for each discretization method. The form asks for personal information from the participant(s) as well as for a brief description of the discretization method. After the application has been approved, the researcher will be asked to sign a participation agreement that states that the participant should not publish the results of other people before we do collectively. Once that is signed, the researcher will be granted developer access to the Git repository enabling him/her to download the required input data for the benchmark cases, to view the simulation results of the other participants as well as to upload his/her own results.

5.2 Simulation and synchronization

In this stage, the participant is expected to perform the computations and convert his/her results to the requested format. In particular, he/she should try the proposed scripts to evaluate the data as indicated in each case description. The deadline for uploading the results to the Git repository is 31 January 2019. The participant should follow the GitLab feature branch workflow that consists of contributing additions via a GitLab merge request of a corresponding branch, analogous to the GitHub standard fork and pull request workflow, see the details below in Subsection 5.4. The uploaded results will be visible to all participants. This will initiate a synchronization phase in which we will discuss and potentially recompute/adjust the results. In particular, a minisymposium at the SIAM GS 19 is planned for presenting the benchmark cases, the participants and the participating schemes as well as for discussing the results. The synchronization phase is supposed to be finished by uploading the final results before 15 May 2019.

5.3 Publication

As a final outcome of this benchmark study, we aim for a joint publication in a peer-reviewed top-ranked journal. We would expect from each participant that he/she helps us in writing and evaluating the manuscript before initial submission as well as during the reviewing process. We would like to stress that co-authorship can only be granted for at most two persons per participating discretization method.

5.4 Details on reporting results

All data requested will be collected in the Git repository <https://git.iws.uni-stuttgart.de/benchmarks/fracture-flow-3d.git>. To ensure a unified and streamlined work flow, please observe the following structure and formatting of the uploaded files.

The repository contains one folder for each of the four test cases. In the `results` folder of these, each method will be assigned a folder with the format

```
$ACRONYM_INSTITUTION/$ACRONYM_NUMERICAL_SCHEME/.
```

No white spaces are allowed, please be consistent with upper and lower case. As an example, results for the first test case obtained using the University of Bergen implementation of the Mixed Virtual Element method are stored in `single/results/UiB/MVEM`. Similarly, the string `$ACRONYM_INSTITUTION-$ACRONYM_NUMERICAL_SCHEME` (e.g. `UiB-MVEM`) constitutes an ID to be used in the handling and labeling of the results.

In the `methods` folder, three categories of files should be placed, for which we here specify the format:

1. **Plot over line:** A csv file whose first column contains the arc length and the second column contains the corresponding values for either c or h , sampled at 2k equidistant points along the specified line. The delimiter is a comma and there is no header for the file, an example is

```
0.0, 3.36948657742311
0.5, 5.38490345323433
1.0, 8.34820934803293
```

Generally, the file is called `dol` (data over line). If several refinement levels are reported for the same test case, the files will be distinguished by adding an appendix to the file name, see individual test case descriptions. The plot over line can be easily done with the “Plot Over Line” filter of ParaView, but a rearrangement of the output may be required.

2. **Plot versus time:** A csv file named `dot` (data over time) whose first column contains the time and the subsequent columns contain the values specified in each test case. The same specifications apply as in the previous case.
3. **Cell numbers and other metrics:** A file named `results.csv` where the first four columns contain the total number of cells in Ω_d , $d = 0, \dots, 3$. The next two columns contain the number of degrees of freedom `dof` and the number of non-zero elements in the matrix `nnz`, respectively. These are followed by other metrics in the order specified in the test case descriptions. If results are reported for several refinement levels, the coarsest refinement level corresponds to the first row etc. Again, the delimiter is a comma and there is no header for the file.

Scripts for generating the plots are to be found in the `scripts` folders in each of the test case folders. The scripts are named `pol.py` and `pot.py` and contain comments on how to add new data. Once new results have been generated, first update the Git repository. Add corresponding lines to the plot scripts and upload the scripts and commit the corresponding data files to a newly created feature branch. After pushing to the remote server, you can create a corresponding merge request that will be reviewed and eventually approved by the repository maintainers. Please verify that the scripts are working before pushing to the remote Git repository. More details can be found at <https://docs.gitlab.com/ee/workflow/workflow.html> and <https://docs.gitlab.com/ee/gitlab-basics/add-merge-request.html>.

6 Appendix

6.1 Additional information for the test case of Subsection 4.2

We report the coordinates for the four corners of the fractures

<i>ID</i>	x_0	y_0	z_0	x_1	y_1	z_1	x_2	y_2	z_2	x_3	y_3	z_3
0	0.5	0	0	0.5	1	0	0.5	1	1	0.5	0	1
1	0	0.5	0	1	0.5	0	1	0.5	1	0	0.5	1
2	0	0	0.5	1	0	0.5	1	1	0.5	0	1	0.5
3	0.75	0.5	0.5	0.75	1.0	0.5	0.75	1.0	1.0	0.75	0.5	1.0
4	0.5	0.5	0.75	1.0	0.5	0.75	1.0	1.0	0.75	0.5	1.0	0.75
5	0.5	0.75	0.5	1.0	0.75	0.5	1.0	0.75	1.0	0.5	0.75	1.0
6	0.50	0.625	0.50	0.75	0.625	0.50	0.75	0.625	0.75	0.50	0.625	0.75
7	0.625	0.50	0.50	0.625	0.75	0.50	0.625	0.75	0.75	0.625	0.50	0.75
8	0.50	0.50	0.625	0.75	0.50	0.625	0.75	0.75	0.625	0.50	0.75	0.625

We report the *region_id*

$$\begin{aligned}
 \text{region_id}(x < 0.5 \cap y < 0.5 \cap z < 0.5) &= 0 \\
 \text{region_id}(x > 0.5 \cap y < 0.5 \cap z < 0.5) &= 1 \\
 \text{region_id}(x < 0.5 \cap y > 0.5 \cap z < 0.5) &= 2 \\
 \text{region_id}(x > 0.5 \cap y > 0.5 \cap z < 0.5) &= 3 \\
 \text{region_id}(x < 0.5 \cap y < 0.5 \cap z > 0.5) &= 4 \\
 \text{region_id}(x > 0.5 \cap y < 0.5 \cap z > 0.5) &= 5 \\
 \text{region_id}(x < 0.5 \cap y > 0.5 \cap z > 0.5) &= 6 \\
 \text{region_id}(x > 0.75 \cap y > 0.75 \cap z > 0.75) &= 7 \\
 \text{region_id}(x > 0.75 \cap y > 0.5 \cap z > 0.75) &= 8 \\
 \text{region_id}(x > 0.5 \cap x < 0.75 \cap y > 0.75 \cap z > 0.75) &= 9 \\
 \text{region_id}(x > 0.5 \cap x < 0.75 \cap y > 0.5 \cap y < 0.75 \cap z > 0.75) &= 10 \\
 \text{region_id}(x > 0.75 \cap y > 0.75 \cap z > 0.5 \cap z < 0.75) &= 11 \\
 \text{region_id}(x > 0.75 \cap y > 0.5 \cap y < 0.75 \cap z > 0.5 \cap z < 0.75) &= 12 \\
 \text{region_id}(x > 0.5 \cap x < 0.75 \cap y > 0.75 \cap z > 0.5 \cap z < 0.75) &= 13 \\
 \text{region_id}(x > 0.5 \cap x < 0.625 \cap y > 0.5 \cap y < 0.625 \cap z > 0.5 \cap z < 0.625) &= 14 \\
 \text{region_id}(x > 0.625 \cap x < 0.75 \cap y > 0.5 \cap y < 0.625 \cap z > 0.5 \cap z < 0.625) &= 15 \\
 \text{region_id}(x > 0.5 \cap x < 0.625 \cap y > 0.625 \cap y < 0.75 \cap z > 0.5 \cap z < 0.625) &= 16 \\
 \text{region_id}(x > 0.625 \cap x < 0.75 \cap y > 0.625 \cap y < 0.75 \cap z > 0.5 \cap z < 0.625) &= 17
 \end{aligned}$$

$region_id(x > 0.5 \wedge x < 0.625 \wedge y > 0.5 \wedge y < 0.625 \wedge z > 0.625 \wedge z < 0.75) = 18$
 $region_id(x > 0.625 \wedge x < 0.75 \wedge y > 0.5 \wedge y < 0.625 \wedge z > 0.625 \wedge z < 0.75) = 19$
 $region_id(x > 0.5 \wedge x < 0.625 \wedge y > 0.625 \wedge y < 0.75 \wedge z > 0.625 \wedge z < 0.75) = 20$
 $region_id(x > 0.625 \wedge x < 0.75 \wedge y > 0.625 \wedge y < 0.75 \wedge z > 0.625 \wedge z < 0.75) = 21$

6.2 Additional information for the test case of Subsection 4.3

We report the coordinates for the four corners of the fractures

ID	x_0	y_0	z_0	x_1	y_1	z_1	x_2	y_2	z_2	x_3	y_3	z_3
0	0.05	0.25	0.5	0.95	0.25	0.5	0.95	2	0.5	0.05	2	0.5
1	0.5	0.05	0.05	0.5	0.05	0.95	0.5	0.3	0.95	0.5	0.3	0.05
2	0.05	1	0.5	0.95	1	0.5	0.95	2.2	0.85	0.05	2.2	0.85
3	0.05	1	0.48	0.95	1.0	0.48	0.95	2.2	0.14	0.05	2.2	.14
4	0.17	1.9	0.7	0.17	1.9	0.3	0.23	2.2	0.3	0.23	2.2	0.7
5	0.23	1.9	0.7	0.23	1.9	0.3	0.17	2.2	0.3	0.17	2.2	0.7
6	0.77	1.9	0.7	0.77	1.9	0.3	0.77	2.2	0.3	0.77	2.2	0.7
7	0.83	1.9	0.7	0.83	1.9	0.3	0.83	2.2	0.3	0.83	2.2	0.7

References

1. Flemisch, B., Berre, I., Boon, W., Fumagalli, A., Schwenck, N., Scotti, A., Stefansson, I. & Tatomir, A. Benchmarks for single-phase flow in fractured porous media. *Adv. Water Resour.* **111**, 239–258 (2018). doi:[10.1016/j.advwatres.2017.10.036](https://doi.org/10.1016/j.advwatres.2017.10.036).
2. Raviart, P.-A. & Thomas, J.-M. A mixed finite element method for second order elliptic problems. *Lect. Notes Math.* **606**, 292–315 (1977).
3. Brezzi, F. & Fortin, M. *Mixed and Hybrid Finite Element Methods*, vol. 15 of *Computational Mathematics* (Springer Verlag, Berlin, 1991).
4. Roberts, J. E. & Thomas, J.-M. Mixed and hybrid methods. In *Handbook of numerical analysis, Vol. II*, Handb. Numer. Anal., II, 523–639 (North-Holland, Amsterdam, 1991). doi:[10.1016/S1570-8659\(05\)80041-9](https://doi.org/10.1016/S1570-8659(05)80041-9).
5. Ern, A. & Guermond, J.-L. *Theory and Practice of Finite Elements*. Applied mathematical sciences (Springer, 2004). URL <http://books.google.it/books?id=CCjm79FbJbcC>.
6. Alboin, C., Jaffré, J., Roberts, J. E., Wang, X. & Serres, C. *Domain decomposition for some transmission problems in flow in porous media*, vol. 552 of *Lecture Notes in Phys.*, 22–34 (Springer, Berlin, 2000). doi:[10.1007/3-540-45467-5_2](https://doi.org/10.1007/3-540-45467-5_2).
7. Faille, I., Flauraud, E., Nataf, F., Pégaz-Fiornet, S., Schneider, F. & Willien, F. A New Fault Model in Geological Basin Modelling. Application of Finite Volume Scheme and Domain Decomposition Methods. In *Finite volumes for complex applications, III (Porquerolles, 2002)*, 529–536 (Hermes Sci. Publ., Paris, 2002).
8. Angot, P. A model of fracture for elliptic problems with flux and solution jumps. *Comptes Rendus Math.* **337**, 425–430 (2003). doi:[10.1016/S1631-073X\(03\)00300-5](https://doi.org/10.1016/S1631-073X(03)00300-5).
9. Martin, V., Jaffré, J. & Roberts, J. E. Modeling Fractures and Barriers as Interfaces for Flow in Porous Media. *SIAM J. Sci. Comput.* **26**, 1667–1691 (2005). doi:[10.1137/S1064827503429363](https://doi.org/10.1137/S1064827503429363).
10. D’Angelo, C. & Scotti, A. A mixed finite element method for Darcy flow in fractured porous media with non-matching grids. *Math. Model. Numer. Analysis* **46**, 465–489 (2012). doi:[10.1051/m2an/2011148](https://doi.org/10.1051/m2an/2011148).
11. Fumagalli, A. & Scotti, A. An Efficient XFEM Approximation of Darcy Flows in Arbitrarily Fractured Porous Media. *Oil Gas Sci. Technol. - Revue d’IFP Energies Nouvelles* **69**, 555–564 (2014). doi:[10.2516/ogst/2013192](https://doi.org/10.2516/ogst/2013192).
12. Schwenck, N., Flemisch, B., Helmig, R. & Wohlmuth, B. Dimensionally reduced flow models in fractured porous media: crossings and boundaries. *Comput. Geosci.* **19**, 1219–1230 (2015). doi:[10.1007/s10596-015-9536-1](https://doi.org/10.1007/s10596-015-9536-1).
13. Flemisch, B., Fumagalli, A. & Scotti, A. *A Review of the XFEM-Based Approximation of Flow in Fractured Porous Media*, vol. 12 of *SEMA SIMAI Springer Series*, chap. Advances in Discretization Methods, 47–76 (Springer International Publishing, Cham, 2016). doi:[10.1007/978-3-319-41246-7_3](https://doi.org/10.1007/978-3-319-41246-7_3).
14. Boon, W. M., Nordbotten, J. M. & Yotov, I. Robust discretization of flow in fractured porous media. *SIAM J. on Numer. Analysis* **56**, 2203–2233 (2018). doi:[10.1137/17M1139102](https://doi.org/10.1137/17M1139102).

15. Fumagalli, A. & Keilegavlen, E. Dual virtual element methods for discrete fracture matrix models. Tech. Rep., arXiv:1711.01818 [math.NA] (2017). URL <https://arxiv.org/abs/1711.01818>.
16. Nordbotten, J. M., Boon, W., Fumagalli, A. & Keilegavlen, E. Unified approach to discretization of flow in fractured porous media. *Comput. Geosci.* (2018). URL <https://arxiv.org/abs/1802.05961>. Accepted.
17. Zielke, W., Helmig, R., Krohn, K., Shao, H. & Wollrath, J. Discrete modelling of transport processes in fractured porous rock. In *7th ISRM Congress*, 57–60 (1991). URL <https://www.onepetro.org/conference-paper/ISRM-7CONGRESS-1991-013>.
18. Barlag, C., Hinkelmann, R., Helmig, R. & Zielke, W. Adaptive methods for modelling transport processes in fractured subsurface systems. In *3rd International Conference on Hydroscience and Engineering, Cottbus* (1998).
19. Geiger, S., Dentz, M. & Neuweiler, I. A novel multi-rate dual-porosity model for improved simulation of fractured and multiporosity reservoirs. *SPE J.* **18**, 670–684 (2013). doi:[10.2118/148130-PA](https://doi.org/10.2118/148130-PA).